Influence of nanoparticles and magnetic surface stress on the emitted beam of an ionic liquid ferrofluid electrospray

IEPC-2017- 285

Presented at the 35th International Electric Propulsion Conference
Georgia Institute of Technology • Atlanta, Georgia • USA
October 8 – 12, 2017

Kurt J. Terhune* and Lyon B. King†
Michigan Technological University, Houghton, Michigan, 49931, USA

Michaël Y. Juillard‡
École Polytechnique de Lausanne, CH-1015, Lausanne, Switzerland

Three solutions of an ionic liquid ferrofluid (ILFF) propellant created by stabilizing nanometer-sized iron oxide particles in 1-ethyl-3-methylimidazolium bis(trifluoromethylsulfonyl)imide (EMIM-NTf2) were electrosprayed from a capillary source. The solutions had 5.98, 8.80, and 11.52 wt% iron-oxide nanoparticles (NPs) making them susceptible to magnetic fields. A Helmholtz coil was used to impose a magnetic stress on the source. A retarding potential analyzer and a stack of three concentric Faraday plates with decreasing aperture diameters were placed downstream of the source to measure the divergence and energy of the electrospray beam. Beam divergence was highly influenced by the wt% NPs in the ILFF even without application of a magnetic field. The addition of NPs reduced the overall beam energy of the source. When a magnetic field was applied, the magnetic stress was observed to decrease the beam divergence and increase the beam energy. The effect of the former was only significant for the 5.98-wt% and 8.80-wt% NPs propellants. The magnetic stress increased the beam energy of all ILFF propellants between 2% and 16% of the beam energy when compared to the zero-magnetic-stress electrospray. The magnetic influence is hypothesized to come from a change in the Taylor cone-jet structure and not from free-space perturbation of emitted particles.

Nomenclature

a	=	Helmholtz coil radius
B	=	magnetic field strength
e	=	elementary charge
$\langle \epsilon_{ion} \rangle$	=	most probable ion energy
η_B	=	beam divergence efficiency
η_V	=	voltage utilization efficiency
H	=	magnetic field
I	=	Helmholtz coil current
$J(\theta)$	=	ion current density as a function of beam half-angle

* PhD Candidate, Department of Mechanical Engineering – Engineering Mechanics, kjterhun@mtu.edu
† Professor, Department of Mechanical Engineering – Engineering Mechanics, lbking@mtu.edu
‡ Graduated with Masters in Electronics and Microelectronics, michael.juillard@epfl.ch

K = electrical conductivity
μ_0 = magnetic permeability
M = magnetization of the fluid
n = number of coil wraps of Helmholtz coil
Q = volumetric flowrate
r = radius from the center of electrospray beam-axis
θ = beam half-angle
$\bar{\theta}$ = average ion trajectory half-angle
V_{ext} = extraction potential

I. Introduction

WITH the acceleration of CubeSat development comes the necessity for the study and development of small propulsion devices.[1-3] Electrospray propulsion is one candidate technology that may be functional for small satellites while also being scalable for use on larger spacecraft.[4-8] An electrospray jet is formed when a conducting or polar liquid is crafted into a sharp point by an underlying solid structure, such as a capillary tube or needle tip, and an electric field is used to extract a beam of charged particles. In spacecraft propulsion, the fluid, referred to henceforth as the propellant, is typically part of a family of fluids called ionic liquids (ILs), which can be tailored to be highly-conductive with near-zero outgassing and so well suited for vacuum environments.[7, 9, 10]

Extensive research and development of electrospray thrusters has been accomplished using multiple propellants.[6, 11-17] Many of the studies focused specifically on the electrospray beam, including its shape, composition, and temperature, quantities that are helpful in uncovering the operational physics. Simply changing the IL propellant can have drastic effects on the electrospray beam, including how wide the plume is,[18] or whether it emits droplets, ions, or a mixture of the two.[19]

One unique type of electrospray propellant that has been studied is an IL-based ferrofluid. Several different varieties of ionic liquid ferrofluids (ILFFs) – Ethylammonium nitrate (EAN),[20] 1-Ethyl-3-methylimidazolium bis(trifluoromethylsulfonyl)imide (EMIM-NTf2),[21-26] and sulfolane/EAN mixture[27] - have been electrosprayed from two different sources: a capillary electrospray source and an ILFF-peak electrospray source developed using the magnetically-induced Rosensweig instability.[20, 28] The studies using ILFFs have examined the stability regime – extraction potentials (V_{ext}) and flowrates (Q) for stable emission – of both sources, and their subsequent emission current, measured the onset potential of the sources, measured specific masses within the electrospray beams of the sources, and performed limited characterization of the electrospray beam.[22] Work reported here expands on the available measurements of beam properties.

II. Goal of Study

ILFF electrospray differs from its classical counterpart both because the sprayed 'fluid' is a colloid consisting of two distinct phases, and because the now-superparamagnetic fluid is subject to strong magnetic stresses at the meniscus. The goals of this study were twofold: 1) Quantify how or if the presence of solid nanoparticles within an ionic liquid affect the divergence and energy of an ILFF electrospray beam; and 2) Measure the influence of magnetic stress on the divergence and energy of an ILFF electrospray beam.

III. Background

A. Efficiency of Electrospray Thrusters

An important parameter of an electrospray thruster is the efficiency in which the device converts propellant and power into change in velocity of the spacecraft. The thruster efficiency is estimated by determining the inefficiencies resulting from multiple operating characteristics of a thruster. Two characteristics of electrosprays measured in this study are beam divergence and beam energy, with respective efficiencies of beam divergence efficiency, η_B, and voltage utilization efficiency, η_V.

The beam divergence efficiency, η_B, is dependent on the angle of off-axis trajectories of emitted charged particles (ions and/or droplets) and is determined using a weighted distribution function of the ion current density, $J(\theta)$, which is angular dependent,

$$\eta_B = \left\langle \cos\bar{\theta} \right\rangle^2 = \left[\frac{\int \cos\theta J\ \ \theta\ \ r^2 \sin\theta d\theta}{\int J\ \ \theta\ \ \sin\theta d\theta} \right]^2 . \quad (1)$$

Here, θ is the half angle at which the current density is measured, r, is the radial distance from the center beam axis, and $\bar{\theta}$ is the average ion trajectory half-angle.

The voltage utilization efficiency is the percent of the extraction potential, V_{ext}, through which the emitted charged particles are accelerated. It is expressed as,

$$\eta_V = \frac{\frac{1}{2} m \left\langle v^2 \right\rangle}{eV_{ext}} . \quad (2)$$

where $\frac{1}{2} m \left\langle v^2 \right\rangle = \left\langle \epsilon_{ion} \right\rangle$, the most probably ion kinetic energy. The η_V of a device can be determined in a laboratory setting through the measurement stopping potential of emitted charged particles from the device (*i.e.* beam energy) using a RPA.

B. Electrospray Beam Diagnostics

Multiple diagnostic tools exist to measure beam divergence ranging in collection method and angular resolution. Lozano developed a current collector comprised of 10 concentric rings (largest had a 6-cm diameter) and a center circular plate to measuring beam spread/focusing.[29] He found that the collector needed to be positioned relatively close to the source (within 7-cm) to collect the majority of the electrospray beam.

Prince's group at the Air Force Research Laboratory attached their capillary electrospray source to a rotatable platform such that it could rotate ±45° in the vertical plane.[30] They collected beam current profiles by measuring the emitted current on a downstream Faraday cup as they rotated the source. Similarly, a Massachusetts Institute of Technology team led by Gassend developed a method of rotating a 2-dimensional array of electrospray emitters to measure divergence of the beam along two-axes.[31] The advantages of these setups over Lozano's was their ability to gather current profiles over a large angular range without requiring the close proximity of the diagnostic tool to the source.

The diagnostic typically used to measure the energy of electrosprayed species is a retarding potential analyzer (RPA). A description of RPA function is presented well by Hutchinson.[32] Variations of RPAs have been designed and tested for electrospray devices. Miller et al. used a set of three grids each in line with the far-field electrospray beam axis and measured the potential required to block ions from entering the main detection unit of their time-of-flight (TOF) mass spectrometer.[30] Lozano used a similar method in a linear TOF mass spectrometer wherein two parallel grids were placed before the TOF collector and biased to an increasing potential until zero current was measured.[29] Most recently, a spherical RPA was developed by Miller et al to measure the fragmentation rates of ion clusters.[33] Her design was specifically crafted to mitigate IL buildup on the RPA grids, a common failure mechanism of RPAs when measuring IL electrosprays.

IV. Equipment and Facilities

The equipment required to complete the goals of this study are described in sections A through F. This includes the design and construction of the ionic liquid capillary electrospray source (IF-CES), the Faraday stack, and the experiment-specific RPA. All experiments were conducted in the ultra-high vacuum (UHV) facility in the Ion Space Propulsion Laboratory (Isp Lab) at Michigan Technological University.

A. Ionic Liquid Ferrofluid Capillary Electrospray Source

The design for the IF-CES (Fig. 1) was based on apparatuses used by Chiu et al.,[34, 35] Lozano et al.,[29] and Miller et. al.[30, 36, 37], which used a glass capillary needle as the emitter, and fed ionic-liquid propellant to the needle apex using either a syringe pump or pressurized vial. The IF-CES included a 0.50-m or 0.75-m long, 75-µm-inner-diameter capillary needle with a wall thickness of ~5 µm at the apex, and the IL or ILFF propellant was fed by a pressure-feed system that is described in literature.[24] A constant-inner-diameter capillary needle, in contrast to tapered-inner-diameter needles used in literature, was selected to counter blockage issues observed in preliminary tests. The completed apparatus included an aluminum extractor plate with a 1.5-mm-diameter aperture to permit electrospray emission from the capillary needle, a PTFE block to both hold and isolate the needle, and set screws to align the needle apex with the extractor aperture.

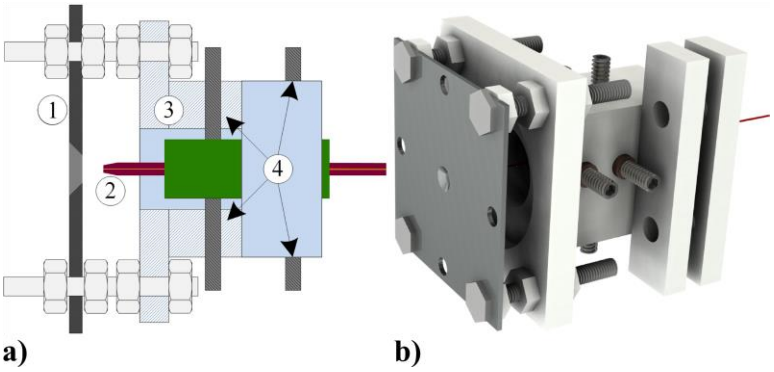

Figure 1. a) Capillary electrospray source comprised of (1) extractor plate, (2) capillary needle, (3) PTFE isolation block, (4) alignment set screws. b) CAD model of IF-CES.

B. Propellants

Four propellants were used in this experiment; the neat IL EMIM-NTf2 (by neat, meaning no nanoparticles), and four solutions of an EMIM-NTf2-based ILFF with varying concentrations of magnetic nanoparticles. The ferrofluids are henceforth called ILFF-20, ILFF-30, and ILFF-40 based on the volume percent of the parent ILFF that was mixed with neat IL. The parent ILFF contained 26.0 wt% iron oxide nanoparticles which led to nanoparticle concentrations in the three solutions of 5.98, 8.80, 11.52 wt% for ILFF-20, ILFF-30, and ILFF-40, respectively. The ratio of ILFF to neat IL used to produce each solution, along with the nanoparticle concentration and fluid density of each solution are tabulated in Table 1.

Table 1. Properties of all propellants used in the experiments.

ILFF Dilution	Ratio ILFF:neat IL	Nanoparticle Concentration, % wt/wt	Density, g/ml
Neat IL (EMIM-NTf2)	0:1	0.00	1.523
ILFF-20	1:4	5.98	1.58
ILFF-30	3:7	8.80	1.61
ILFF-40	2:3	11.52	1.63

C. Ultra-High Vacuum Facility

The ultra-high vacuum (UHV) facility (Fig. 2) is approximately 0.5 meters in diameter and 0.5 meters in length, with a base pressure of 10E-9 Torr. High vacuum is achieved using a 280 L/s turbo-molecular pump with a 110 L/min backing dry scroll pump; ultra-high vacuum is achieved using a 300 L/s combination ion-sublimation pump.

Other test equipment accessible in this facility includes a Matsusada AMT-5B20 high voltage amplifier capable of ±5 kV output at 20 mA, a Rigol DG4162 arbitrary function generator, EEVBlog µCurrent micro-ammeters, an in-house-built high-voltage uAmmeter, and a Keithley 2410 Sourcemeter. The signals from each piece of

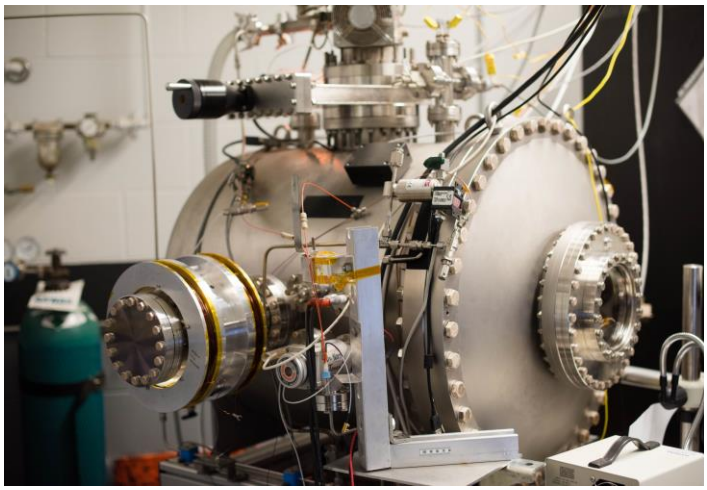

Figure 2. The ultra-high vacuum facility in the Ion Space Propulsion Laboratory at Michigan Technological University.

test equipment can be recorded through an NI PXI-1033 data acquisition chassis via a SCB-68 connector block, or a NI USB-6361 mutlifuction I/O device.

D. Helmholtz Coil

The Helmholtz coil can be seen attached to the UHV facility in Fig. 2. The radius of the coil, *a*, was 9.5 cm; it was selected based on the diameter of the source flange that enclosed the IF-CES. Coil separation of Helmholtz coil was 10 cm. The current, *I*, was bound by the power supplies available for use in the experiments. Therefore, the number of wraps, *n*, was determined by selecting a maximum magnetic field strength, *B*, and solving a variant of Biot-Savart's law, $B = (4/5)^{3/2} \mu_0 nI/a$. The final design had a maximum center-axis magnetic field strength of 200 Gauss when the coils were powered with 5.56 Amps of current at 120-180 V. Excess heat was an expected issue and the coils were either water-cooled using a copper-pipe sleeve that fit between the coil and the flange, or cooled via forced-air convection using a box fan, allowing the Helmholtz coil to be operated for minutes at a time.

E. Faraday Stack

The Faraday stack diagnostic built to measure beam divergence of IF-CES consisted of three concentric stainless-steel plates placed along the downstream axis of the electrospray beam, Fig. 3. This design was like Lozano's, albeit fewer concentric plates, and the plates were separated by centimeters to avoid shorting caused by the buildup of IL. It was chosen over a rotatable stage (like that used by Prince's group) since the Helmholtz coil fixed to the facility and could not be rotated with the source. The large-aperture Faraday plate (LRP) was placed 28.2-mm downstream of the extractor plate and had an 18.1-mm -diameter of aperture; the small-aperture Faraday plate (SMP) was 41.75-mm downstream of the extractor plate and had a 12.75-mm-diameter aperture; the solid Faraday plate (SFP) was 54.9-mm downstream of the extractor plate. Changes in the current fraction measured on each plate indicate potential tightening or broadening of the beam. The half angle of the electrospray beam that interacted with each Faraday plate was determined by geometry of the setup, i.e. the radii of the apertures in the extractor plate, LRP and SMP, and the distance each was from the source. The emission current was measured via an in-house-built high-voltage μAmmeter, and the current measured on each Faraday plate was measured through three individual EEVblog μCurrent microammeters; the output signals of each ammeter were recorded via an input into a NI-6361 USB DAQ and recorded via a LabVIEW VI.

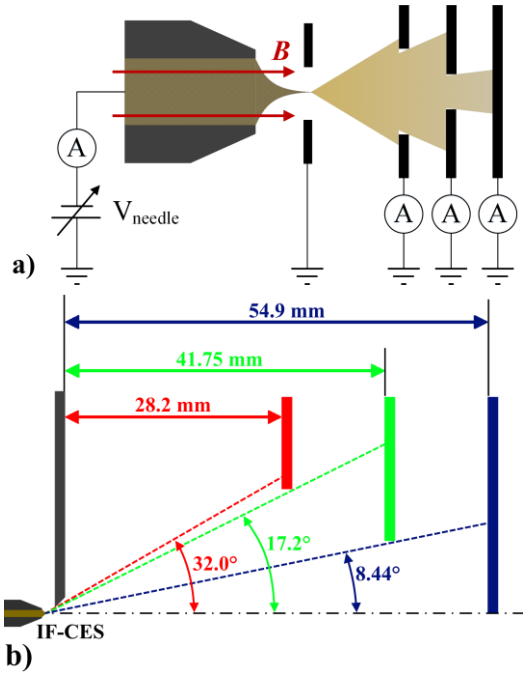

Figure 3. a) Schematic of the Faraday stack used as the beam divergence diagnostic illustrating relative position of the Faraday stack and the circuit design. b) Drawing of Faraday stack with distances from the extractor plate (gray) to the LRP (red), the SMP (green), and the SFP (blue) are denoted. The denoted half-angles represent the portion of the electrospray beam that interacts with each Faraday plate. Not to scale.

F. Retarding Potential Analyzer

An RPA was designed and built to measure the beam energy of the IF-CES electrospray beam based on the criteria of plasma RPAs while also accounting for the differences and obstacles inherent to IL and ILFF electrospray. The final design is shown in Fig. 4. Only two electrostatic grids were used in the design as an electron repeller is not necessary and the secondary electron repeller grid was not included. The grids were constructed from stainless-steel plates with 0.375-in apertures and 20-by-20 wires-per-inch, 0.0118-diameter tungsten wire mesh welded to the back face of each. A 0.50-inch disk was used as the Faraday plate. The two grids and Faraday plate were isolated from each other using 0.175-inch-thick blocks of Delrin® Acetal plastic. The Faraday plate was also seated in a block of Delrin to electrically isolate it from the background environment. The assembly was aligned via alumina rods, and fastened together via stainless-steel rods and nuts sleeved in alumina. The entrance plane of the RPA was 28.3 mm downstream of the IF-CES. The grids were biased using two high-voltage amplifiers with potential signals outputted from a NI-6361 USB DAQ. The input signals for the grid potential, and the output signal from the Faraday plate were input into, and recorded through, an Oscilloscope.

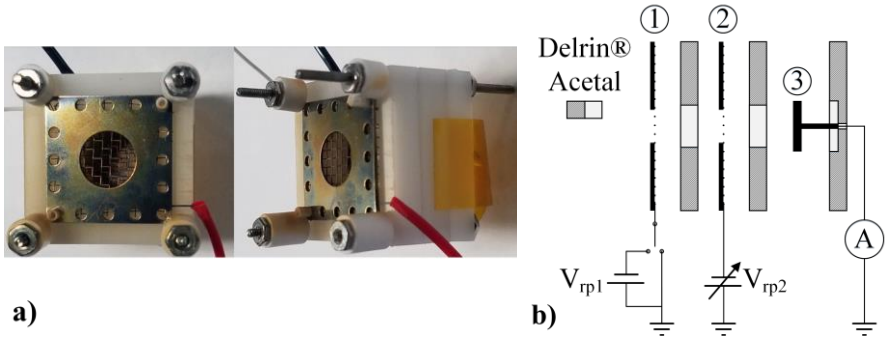

Figure 4. a) Image of the RPA design as a diagnostic of IL and ILFF electrospray b) Circuit schematic of the RPA used in the beam energy diagnostic (exploded view); (1) Front grid, (2) Repeller grid, (3) Faraday plate.

V. Experimental Procedures

The beam divergence of the IF-CES was measured through the following procedure. The IF-CES with the Faraday Stack attached was inserted into the UHV facility and a stable electrospray was established using the neat IL propellant with a flowrate of 0.315 nl/s and an extraction potential of 1400 V. A 200-Gauss magnetic field was then applied to the source for 20 seconds and then removed. The collected-current telemetries on the LRP, SMP, SFP were measured and recorded throughout testing. The entire procedure was repeated for select combinations of flowrate and extraction potential using the neat IL, ILFF-20, ILFF-30 and ILFF-40 propellants, Table 2.

Table 2. Operation settings for the beam divergence experiment.

		Extraction Potential, V						
Propellant		1400	1500	1600	1700	1800	1900	2000
neat IL	**Flowrate, nl/s**	0.315 0.63	0.315 0.63 0.945	0.315 0.63 0.945				
ILFF-20				0.47 0.705	0.47 0.705 0.94	0.47 0.705 0.94		
ILFF-30				0.454	0.454 0.636	0.636 0.818	0.636 0.818	0.636 0.818
ILFF-40					0.47	0.47 0.62 0.78	0.47 0.62 0.78	0.62 0.78

Beam energy for the center axis of the electrospray was measured through the following steps. The IF-CES, with RPA attached downstream, was inserted into the UHV facility. The front grid and repeller grid of the RPA were initially biased to 2000 V to prohibit the electrospray beam from coating the device interior causing electrical shorts

(this is also the state of the plates during non-measurement periods). A stable electrospray was then established using the neat IL propellant at a flowrate of 0.315 nl/s and an extraction potential of 1400 V. Two energy traces were collected by grounding the front RPA grid, and then sweeping the repeller grid from 2000 V to 0 V at a slew rate of 200 V/second. After the sweep, the bias of both RPA grids was returned to 2000 V. A 200-Gauss magnetic field was then applied to the source using the Helmholtz coil, two energy traces were recorded, and then the magnetic field was removed. A total of 10 energy traces for this flowrate and extraction potential were captured, in the sequence of two with a 0 Gauss magnetic field applied to the source, two with 200 Gauss, two with 0 Gauss, two with 200 Gauss, and two with 0 Gauss. The entire procedure was repeated for select combinations of Q and V_{ext} using the neat IL, ILFF-20, ILFF-30 and ILFF-40 propellants. The combinations of Q and V_{ext} for each propellant, along with the maximum front grid potential and the maximum repeller potential are given in Table 3.

Table 3. Operating parameters of the IF-CES during beam energy diagnostics. Repeller potential is the electrical bias potential for both the front grid and repeller plate prior to collecting an RPA sweep.

neat IL	Extraction Potential, V	1400	1500	1600	1700				
	Repeller Potential, V			2000					
	Flowrate, nl/s	0.315, 0.63	0.315 0.63 0.945	0.315 0.63 0.945	0.945				
ILFF-20	Extraction Potential, V		1500	1600	1700	1800	1900		
	Repeller Potential, V			2000		2100			
	Flowrate, nl/s		0.47	0.47, 0.705	0.47 0.705 0.94	0.47 0.705 0.94	0.94		
ILFF-30	Extraction Potential, V			1600	1700	1800	1900	2000	2100
	Repeller Potential, V			2000		2100			2200
	Flowrate, nl/s			0.454	0.454	0.454 0.636 0.818	0.454 0.636 0.818	0.454 0.636 0.818	0.818
ILFF-40	Extraction Potential, V				1700	1800	1900	2000	2100
	Repeller Potential, V				2100		2200		2300
	Flowrate, nl/s				0.47	0.47 0.62 0.78	0.47 0.62 0.78	0.62 0.78	0.78

VI. Results and Discussion

The results from the beam diagnostics on the IF-CES conducted via the procedures in section V, and a discussion on the relevant observations and findings are provided below. The section begins with the results from the beam divergence experiment, beginning with those from neat IL control tests, and followed by those concerning the influence of nanoparticles and then magnetic stress. The section ends with results from the beam energy experiment following the same structure.

A. Neat Ionic Liquid Electrospray Beam Divergence

Figure 6 a) provides an example of the telemetries collected from the beam divergence experiment using neat IL as the propellant. The telemetries are for the emission current of the source and the currents intercepted by each of the Faraday plates, and include operation of the IF-CES with and without a 200-Gauss magnetic field. The extractor plate current was not collected for the experiment; instead the fraction of emission current that was not collected on the three Faraday plates was assumed to have been stopped by the extractor plate.

Figure 5 b) reveals that the flowrate had significant influence on beam divergence of the neat IL electrospray. An increase in flowrate induced an increase in the percent of total emission current measured on both the SMP and LRP,

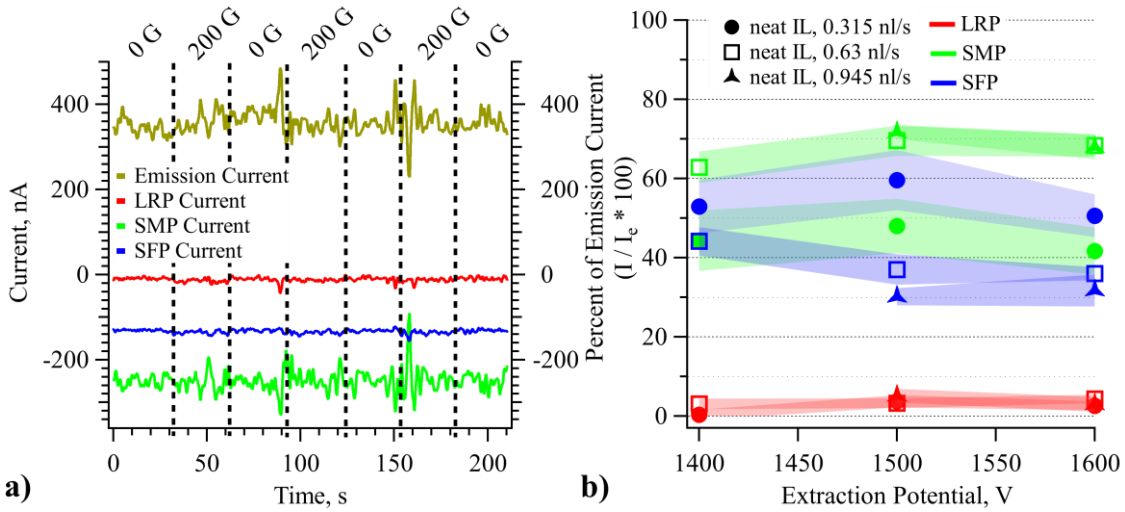

Figure 6. a) Telemetries of the emission current and the intercepted currents measured on the downstream Faraday plates of the IF-CES operating on neat IL at Q = 0.63 nl/s and V_{ext} = 1500 V. The magnetic field strength applied to the IF-CES is denoted at the top of each plot; dashes lines indicate temporal bounds of the applied magnetic field. b) The mean measured current collected on the LRP (red), SMP (green), and SFP (blue) as a percentage of the total emission current plotted against the extraction potential of the IF-CES operating on neat IL at three flowrates. Error is one standard deviation of the percent of emission current.

while reducing the percent of total emission current measured on the SFP. Quantitatively, a 100-percent increase in flowrate reduced the current of the center beam (half angle of 8.44°) by 10- to 20-percent depending on the extraction potential. The center beam current was reduced ~5-percent further with another 50-percent increase in flowrate. The current measured on the SFP is decreased 15- to 25-percent with the initial 100-percent increase in flowrate, and was not significantly changed by any further increase in flowrate. The current measured on the LRP was only significantly increased (3-percent) through a 100-percent increase in flowrate while operating at an extraction potential of 1400 V. Error bars shown in Figure 6 b) are one standard deviation of the mean current. These results suggest the electrospray beam structure underwent a significant change in the angular-current profile.

As the surface areas of each of collector plates LRP, SMP, and SFP were not equivalent, angular-resolved profiles were not an appropriate measure of divergence. Instead the current density as a function of angle was determined by dividing the measured currents on each plate by their respective collection surface area, Fig. 6. The collection surface

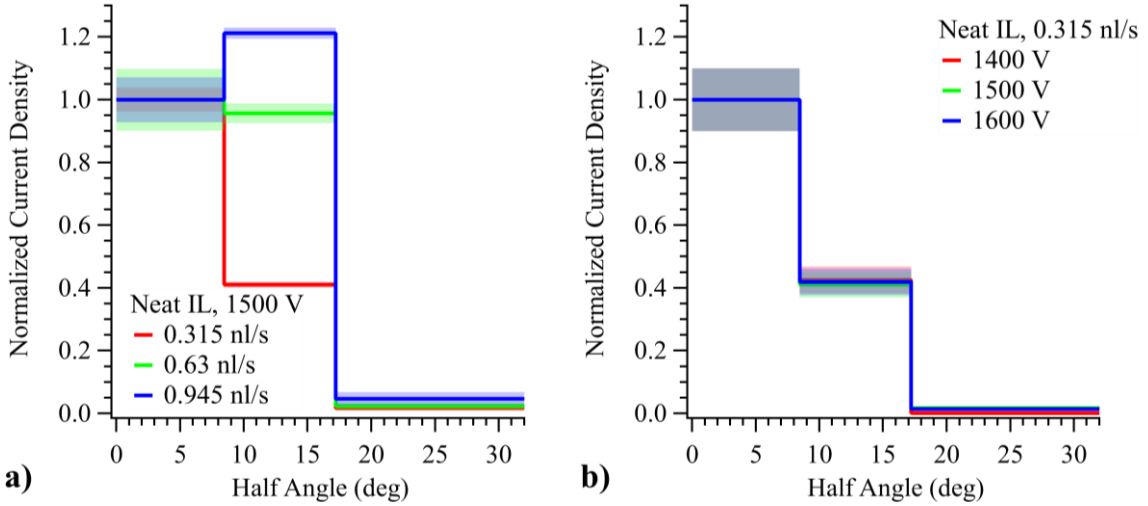

Figure 5. Normalized current density profile of the IF-CES operating on neat IL with a) an extraction potential of 1500 V and flowrates 0.315, 0.63, and 0.945 nl/s, b) with a flowrate of 0.315 nl/s and extraction potentials 1400 V, 1500 V, and 1600 V. The SFP, SMP, LRP are between half-angles 0° - 8.44°, 8.44° - 17.2°, and 17.2° - 32.0°, respectively. Error is one standard deviation of the mean normalized current density.

area was defined as that visible from the source via line-of sight, thus the outer radii of the surface area are at half-angle 32.0°, 17.2°, and 8.44° as shown in Fig. 3 b). The resultant current density profile was then normalized by the current density measured on the SFP, since we were only interested in changes in divergence.

Figure 5 provides the current density profiles measured during IF-CES operation plotted against the beam half-angle. The stepped-shaped of them is the result of only recording a single current across the angular range of each Faraday plate; the SFP is between half-angles of 0° – 8.44°, the SMP is between half-angles of 8.44° – 17.2°, and the LRP is between half-angles 17.2° – 32.0°. Error bars shown in Fig. 6 are on standard deviation of the mean current density.

Figure 5 a) illustrates an increase in the current density between half-angles of 8.44° and 32.0° (corresponding to the collection areas of the SMP and LRP Faraday plates) when the flowrate is increased. Figure 5 b) illustrates that the extraction potential of the IF-CES has no significant influence over the beam divergence. The combined observations in Fig. 6 suggests that the beam broadens only during an increase in flowrate. Similar observations are reported for electrospray sources running, [EMIM][NTf2] propellant,[38] [Bmim][DCA] propellant,[30] and [Emim][EtSO4]-HAN propellant.[17]

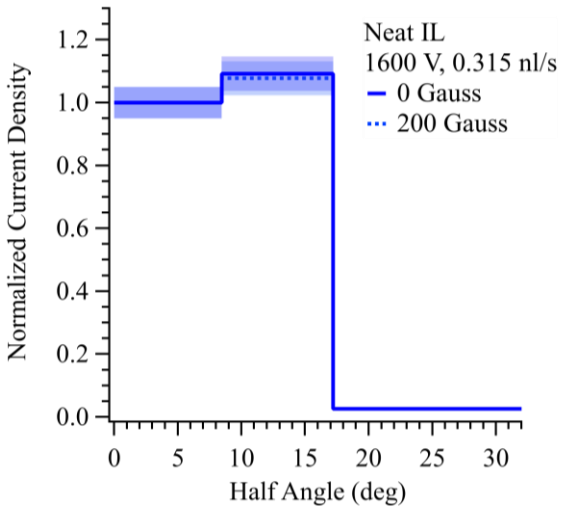

Figure 7. Normalized current density profiles of the IF-CES operating on neat IL with a Q = 0.945 nl/s and V_{ext} = 1600 V, with (dashed line) and without (solid line) a 200-Gauss magnetic field applied. Error is one standard deviation of the mean normalized current density.

Lastly, a 200-Gauss magnetic field was also applied to the neat IL electrospray, and through the comparison between the current density curves with and without the magnetic field we concluded the magnetic field garnered no significant influence on the beam divergence, Fig. 7. Therefore, any subsequent change in beam divergence of ILFF electrosprays can be attributed to the magnetic susceptibility of the propellants. Error bars shown in Fig. 7 are one standard deviation of the mean current density.

From the combined results of Fig. 6 and 7 we concluded that the IF-CES operating on neat IL propellant behaved similarly to other capillary electrospray sources in literature. Therefore, they were used as a control source for the results presented in the following sections, which discuss if/how the new magnetically susceptible propellants changed the beam divergence of the control IF-CES electrospray.

B. Nanoparticle Influence on Beam Divergence of Magnetic-Field-Free ILFF Electrospray

No literature was found that addressed the effect colloidal particles have on the divergence of an electrospray beam. However, in a study by Gamero-Castaño which examined the temperature effects on the expansion of an EMIM-NTf2 electrospray beam, he showed that a 20°C increased the half-angle of the electrospray beam by 85.7% (21- to 39-degrees).[18] He concluded that the temperature induced beam expansion by changing the electrical and liquid properties of the EMIM-NTf2. Other researchers have shown that the temperature of the fluid inherently changes properties of an IL propellant. Specifically, a 20°C increase in temperature from RT induces a 1.3% drop in density, a 49.7% drop in viscosity, a 1.6% increase in surface tension, and a 134.8% increase in conductivity of EMIM-NTf2.[39-41] The ILFF propellants used in this study have different electric and liquid properties induced through the addition of NPs to EMIM-NTf2. Specifically, an increase in wt% NPs increases the density and viscosity, and decreases the surface tension and conductivity of the propellant, Table 4.[24] However, since the effects related to specific liquid properties were not determined in literature, and given the added variable of NPs used in this study, the results in this study could not be compared to literature. As such, the results on the measured effects of the

Table 4. Measured* and interpolated^ liquid and electrical properties of the propellants used in the experiments.

ILFF Dilution	Viscosity, mN/m	Conductivity, S/m	Surface Tension, mPa•s
Neat IL (EMIM-NTf2)	35.8*	0.91*	36.28*
ILFF-20	45.4*	0.83^	35.39^
ILFF-30	58.5*	0.795^	34.96^
ILFF-40	66.0*	0.76^	34.56^

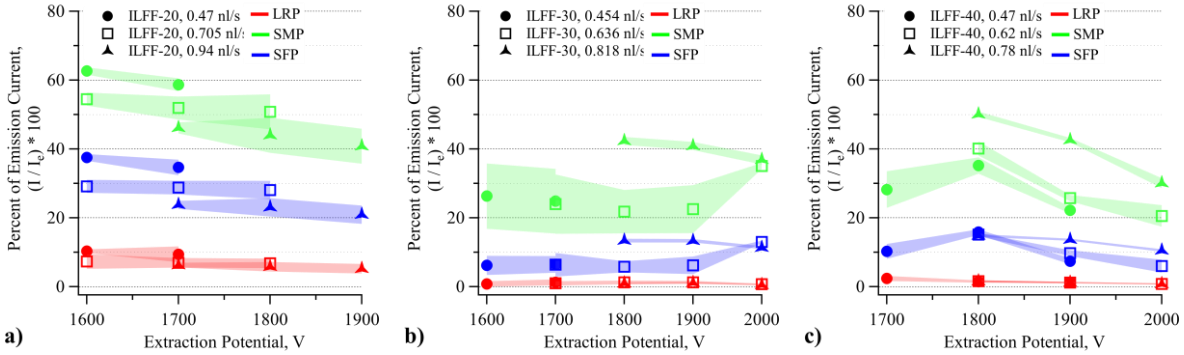

Figure 9. The mean measured current collected on the LRP (red), SMP (green), and SFP (blue) as a percentage of the total emission current plotted against the extraction potential of the IF-CES operating at three flowrates operating on a) ILFF-20, b) ILFF-30, and c) ILFF-40. Error is one standard deviation of the percent of emission current. The electrosprays were not subjected to a magnetic field.

beam divergence in this section are only comparable between the propellants used in this study.

Current telemetries collected from beam divergence experiment using the ILFF propellants were analyzed in a similar manner as those from the neat IL. As with neat IL, the extractor plate current was not collected for the experiment, but instead the fraction of emission current that was not collected on the three plates was assumed to have been stopped by the extractor plate. The results from the beam divergence experiment reveal that an addition of, and subsequent increase in concentration of NPs in neat IL significantly changed the fraction of emission current that was measured on each downstream plate, Figs. 8 and 9.

The mean current collected on each of the Faraday plates as a percent of emission current for all ILFF propellants shown in Fig. 8 reveals that the flowrate also had significant influence on magnetic-field-free ILFF electrosprays. Furthermore, unlike analogous neat IL results (Figure 6 b)), the extraction voltage also affects the percent of the emission current collected on the Faraday stack. Whereas the total fraction of the emission current intercepted by the Faraday plate during neat IL electrospray operation was invariant of the extraction potential, an increase in extraction potential of the source running on ILFF-20 or ILFF-40 corresponded to a decrease in the total fraction of emission current from all three plates; ILFF-30 propellant was invariant to extraction potential. Quantitatively, the total amount of current intercepted by all three Faraday plates when the source operated on neat IL was approximately 100-percent of the emission current, while the total amount of current intercepted by the three Faraday plates when the source operated on the ILFF propellants was typically less than 100-percent of the emission current. Note: at times the data reports over 100-percent on the emission current, however it was always less than 110-percent of the emission current and is most likely a systematic error of the high voltage ammeter.

A change in flowrate affected each ILFF propellant differently. As seen in Fig. 8 a), the fraction of the emission current intercepted by the LRP, SMP, and SFP using the ILFF-20 propellant decreased with an increase in flowrate.

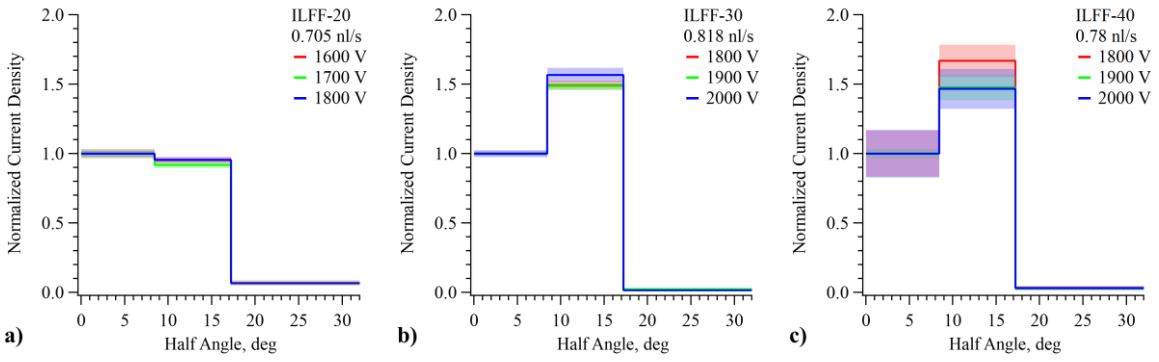

Figure 8. Normalized current density profile of the IF-CES plotted against the half-angle of downstream beam, where 0-degrees is the electrospray beam center axis. a) ILFF-20, b) ILFF-30 and c) ILFF-40 propellants. The increase in wt% NPs in the neat IL from a) to c) is correlated to an increase in beam divergence, ie the relative current density at higher half angles increases from a) to c). Error is one standard deviation of the mean normalized current density.

The fraction of emission current intercepted by the LRP, SMP and SRP using ILFF-30 and ILFF-40 propellants (Fig. 8 b) and c), respectively) either remain constant or decreased with an increase in flowrate. Quantitatively, the current intercepted by the Faraday stack when the source operated on ILFF-20 at Q = 0.47 nl/s was approximately 100-percent of the emission current; at Q = 0.94 nl/s the total current measured on the Faraday stack was between 68 and 76 percent of the emission current. When the source operated on ILFF-30 or ILFF-40 propellants the total current on the Faraday stack as a percent of emission current was considerably reduced; it was 29- to 57-percent for ILFF-30 at flowrates of 0.47 and 0.818 nl/s respectively, and between 27- to 67-percent for ILFF-40, for flowrates of 0.47 and 0.78 nl/s, respectively.

The significant decrease in the total fraction of the beam intercepted by the three Faraday plates is indicative of a reduction in the current traveling within the portion of the electrospray beam intercepted by the Faraday stack. This reduction may be the consequence of an increasingly divergent electrospray beam wherein a larger fraction of the current was at half-angles greater than those collected by the LRP (θ > 32.0°). Alternatively, the beam may be increasingly blocked by the extractor plate. However, each of these possibilities cannot be confirmed as the current was not measured on the extraction plate, and the largest half-angle captured by the LRP is 32.0°.

The fraction of the emission current of the source that was not intercepted by the extractor plate (un-intercepted current fraction) was not directly tied to the weight-percent NPs in the IL, i.e. the un-intercepted current fraction was the smallest for the source operating on the ILFF-30 propellant, not ILFF-40. The cause of this observation was not determined, though it may be the result of the NPs interfering with the emission process differently for each of the solutions.

The current density profiles for each ILFF electrospray at various operating settings (V_{ext}, Q) were calculated using the same method used for the current density profiles of the neat IL, Figs 6 and 7, to compare and quantify the nanoparticle influence on beam divergence. A selection of them for constant Q and three V_{ext} for each ILFF propellant are shown in Fig. 9 to illustrate the effect of the V_{ext} on the beam divergence. Figure 9 a) and b) show that V_{ext} was insignificant to the beam divergence of ILFF-20 and ILFF-30 electrosprays. However, Fig. 9 c) shows that an increase of 100-V in V_{ext} shifted the current density profile of ILFF-40 electrosprays towards the center of the beam; this may come from the extraction potential changing the cone shape, as described by Morad et al.,[42] but no images of the Taylor cone were taken during the experiment to verify this hypothesis. No other statistically significant results exist that show a dependence on V_{ext} but, this could be due to the uncertainty in the current density profile (error shading in Fig. 9) which stemmed from fluctuations in the emission current, Fig. 10 a).

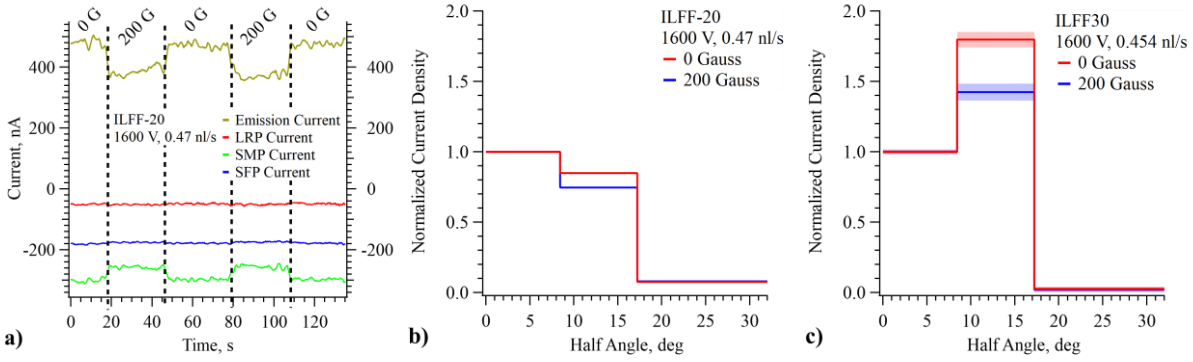

Figure 10. a) Telemetries of the emission current and the intercepted currents measured on the downstream Faraday plates of the IF-CES operating on ILFF-20 at Q = 0.47 nl/s and V_{ext} = 1600 V. The magnetic field strength applied to the IF-CES is denoted at the top of each plot; dashes lines indicate temporal bounds of the applied magnetic field. b) Normalized current density profiles of the IF CES plotted against the half-angle of an ILFF-20 electrospray running at Q = 0.47 nl/s and V_{ext} = 1600 V, and c) Normalized current density profiles of the IF CES plotted against the half-angle of an ILFF-30 electrospray running at Q = 0.454 nl/s and V_{ext} = 1600 V. Error is one standard deviation of the mean normalized current density. 0-degrees is the electrospray beam center axis.

C. Magnetic Influence on Beam Divergence

The current telemetries of the ILFF-20 electrospray operating at 0.47 nl/s reveal that the magnetic field has significant influence on the emission current and the SMP current, Fig 10 a). A possible reason that only the SMP was affected by the magnetic field application was that it had a larger collection area than the SFP, and was located at

lower half-angles than the LRP. This meant the SMP collected the highest current fraction of the electrospray beam relative to the emission current. Thus, any change in emission current is most readily seen in the SMP. Furthermore, the SMP current appears to be the most affected in the current density profiles of Fig. 10 c) and d), due to the normalization of each profile to the current density of the SFP.

The magnetic field influence on beam divergence was quantified by analyzing the current densities of the ILFF-20 and ILFF-30 electrosprays with and without a 200-Gauss magnetic field applied to the source. As Fig. 10 b) and c) show, subjecting the electrospray to the magnetic field acts to constrict the electrospray beam, i.e. the current density at larger half-angles is reduced relative to the current density at smaller half-angles when 200 Gauss is applied to the electrospray. This is only statistically evident for several operating conditions of the IF-CES running on ILFF-20 and ILFF-30.

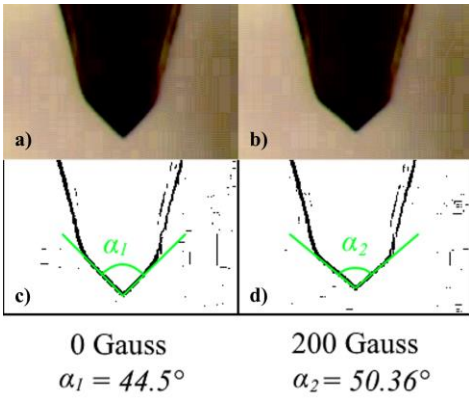

Figure 11. Images of the Taylor cone geometry at the emission site of IF-CES operating on the parent ILFF with an applied magnetic field strength of a) 0 Gauss and b) 200 Gauss. Image enhanced using an edge detector and the cone angle was measured for a magnetic field of c) 0 Gauss and d) 200 Gauss.

Literature on the divergence of a ferrofluid electrospray beam completed by Jackson and King found that a non- uniform magnetic field applied to an electrospray of IL with magnetic nanoparticles tightened the beam.[22] Therefore, the expectation was for the beam to tighten. However, further analysis by Jackson and King showed that the free space trajectory perturbation by magnetic forces was inconsequential.[43] Another potential cause of the beam tightening could be the Kelvin force density, $\mu_0 M \nabla H$. However, as the testing was conducting along the center *z*-axis of a Helmholtz coil, $\partial H/\partial z \simeq 0$ and $\partial H/\partial r \simeq 0$, and consequently $\mu_0 M \nabla H = 0$.

If the Lorentz and Kelvin forces on the particles of the emitted beam are not the mechanism for the change in beam divergence, then a change in emission site geometry induced by the magnetic field may be the cause of the change. A separate study by Jackson et al. which examined the onset potential of the parent ILFF demonstrated that a magnetic force changes the geometry of the Taylor cone during capillary emission;[26] an image of this shape change is shown in Fig. 11. This was a consequence of the magnetic normal traction and the fluid magnetic pressure simultaneously acting to change the shape of the cone-jet region of the meniscus. However, in-situ imaging was not feasible during this study due to the Helmholtz coil location, so the effect was not verified for the ILFF solutions. While in-situ imaging was not conducted in the present paper, it is likely that the cone-jet region of the magnetically enhanced sprays differed from that of the purely electric.

D. Neat Ionic Liquid Electrospray Beam Energy

A set of the results from the RPA diagnostic experiment on a magnetic-stress-free neat IL electrospray from the IF-CES are presented in Fig. 12. Figure 12 a) shows the normalized RPA traces of the source emitting a neat IL electrospray at three flowrates, while Fig. 12 b) shows dI/dV of the RPA current traces; i.e. the first derivative of the traces in Fig. 12 a). Figure 12 b) reveals that the IF-CES IL electrospray emits ions with energy that fall within a single energy distribution, regardless of flowrate and extraction potential. These results agree with those of other capillary electrosprays presented in literature.[17, 29, 44] Another observation from Fig. 12 is the tails of the dI/dV distributions had energies higher than V_{ext}. This is observed in literature and is suggested to be the effect of the combined droplet collection from the beam and secondary electron emission.[17, 45]

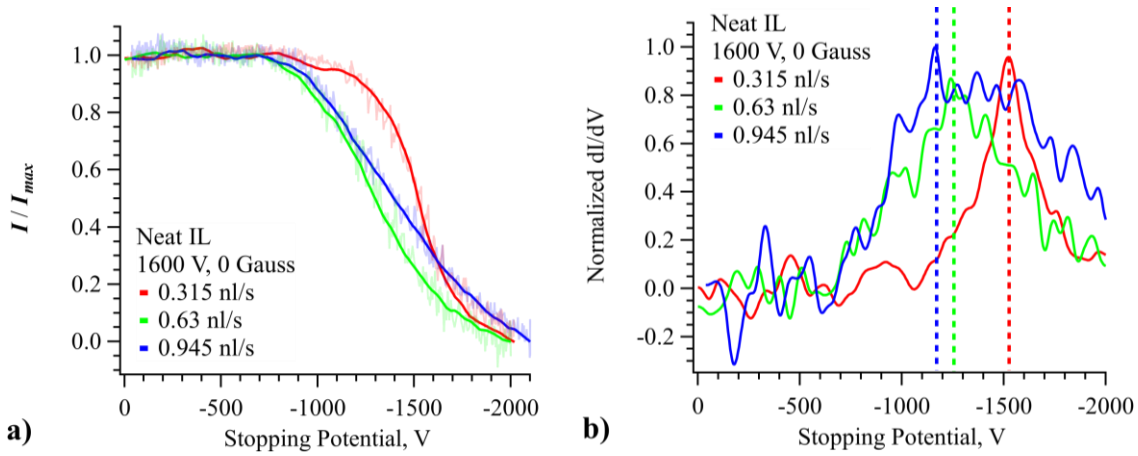

Figure 12. a) RPA traces of neat IL electrospray, and b) normalized derivatives of the same RPA traces; V_{ext} = 1600 V and Q = 0.315, 0.63, and 0.945 nl/s. There was no magnetic field applied to the source in either a) or b).

E. Nanoparticle Influence on Beam Energy

Nanoparticles were observed to have a dramatic effect on the energy distributions of the electrospray beam. The most probable ion energy, $\langle \epsilon_{ion} \rangle$, as a percent of V_{ext} was calculated for multiple (Q,V_{ext}) settings using each of the ILFF electrosprays subjected to zero magnetic stress, Fig. 13. This measurement provides a gauge of the voltage utilization efficiency the IF-CES, as $\eta_V = \langle \epsilon_{ion} \rangle / V_{ext}$. The IF-CES electrospray operates at the highest η_V during low flowrate and high extraction potential, (solid squares in Fig. 14). Similar results are observed in work by Miller et al., wherein they found that the decrease in energy correlated to the cone extending further into the electric field during higher flowrates.[37] Lozano also observed a drop in energy correlated to an increase in flowrate.[29] In both studies the measured energy as a percent of the overall extraction potential is 85- to 90-percent.

The electrospray beam with nanoparticles appeared to be poly-energetic; i.e. two energy distributions existed for electrosprays of the ILFF-30 and ILFF-40 propellants, Fig. 13 b) and c). One above 75-percent of the extraction potential and one below 50-percent of the extraction potential, identified henceforth as the primary and secondary populations, respectively. The energy of the primary population of particles in ILFF electrosprays was similar to those in neat IL electrospray; as Fig. 14

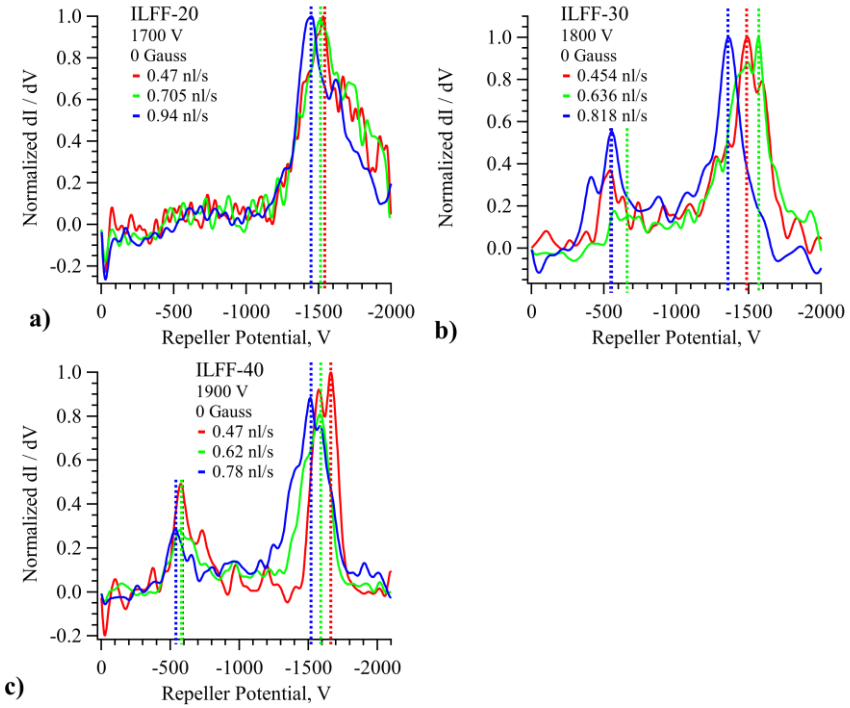

Figure 13. Normalized derivatives of the RPA traces collected from the IF-CES operating on a) ILFF-20, b) ILFF-30, and c) ILFF-40 propellants. There was no magnetic field applied to the source.

shows, η_V of the ILFF electrosprays was 0.75 to 0.9, depending on propellant and flowrate, which is identical to the range for neat IL η_V. Significant flowrate dependence was only observed in the η_V of the primary populations for ILFF-30 and ILFF-40 electrospray, and resulted in a general reduction in beam energy, (green and blue solid square of Fig. 14).

The distinguishing feature between the energy distributions of ILFF and neat IL electrosprays is the secondary population observed when using ILFF-30 and ILFF-40 propellants. These distributions were centered between repeller potentials of -500 to -700 V (or 30- to 50-percent of V_{ext}), Fig. 13 b) and c). As the secondary populations only appeared when the IF-CES was operating on ILFF-30 and ILFF-40, they were likely the result of NPs. However, as the addition of NPs changed the density, surface tension, viscosity and conductivity of the neat IL, (Table 4) and were a physical presence in the spray, the mechanism that produces low energy particles was not differentiated from the other effects of the NPs. A possible mechanism that would produce the secondary population is the fragmentation of ions from the emitted NPs within the extraction field of the source. In a study on the beam energy of an externally wetted EMIM-BF4 electrospray source, Miller and Lozano concluded that similar poly-energetic RPA traces were the result of fragmentation of dimer ion species into monomer species within the extraction field.[33] Thus the lower-energy, secondary populations presented in Fig. 13 could be the consequence of ion species fragmenting from droplets or off of NPs partway through the extraction field of the source. Since this population does not appear in the RPA traces of neat IL or ILFF-20 electrosprays, this hypothesis is possible, but it would require future testing and/or modelling to confirm.

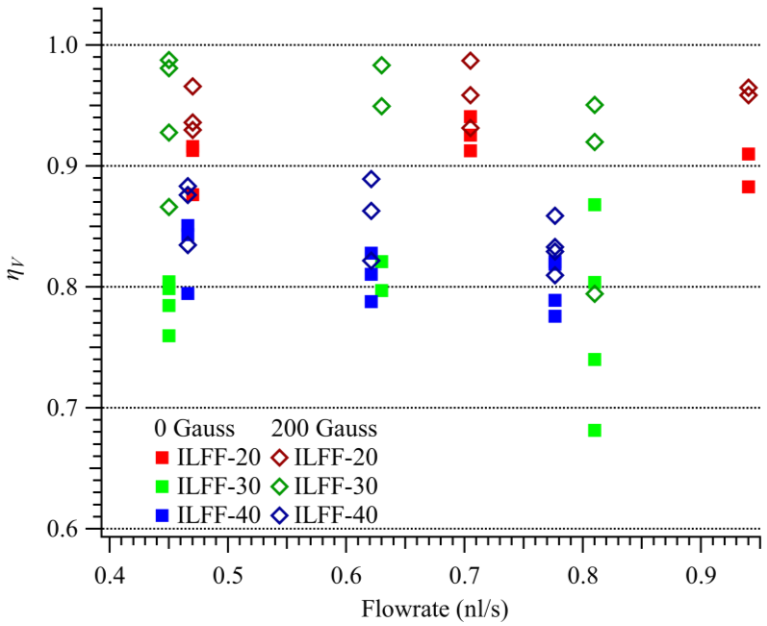

Figure 14. Voltage utilization efficiency for IF-CES operating on ILFF-20, ILFF-30, and ILFF-40 propellants plotted against the *Q*. Error-bars are removed for clarity but are 1 to 4.5 percent change for ILFF-20, 2 to 10 percent change for ILFF-30, and 1.5 to 6 percent change for ILFF-40.

F. Magnetic Influence on Beam Energy

The magnetic influence on the beam energy of the neat IL electrospray was negligible. This was expected as the neat IL propellant was non-magnetic and the effect of the magnetic field on the moving ions emitted from the source was already found to be insignificant (section VI.A.) This provided a baseline for adding magnetic stress to the electrosprays of ILFF propellants.

The magnetic stress significantly influenced the RPA traces collected from the IF-CES operating on the ILFF propellants, Fig 15. Furthermore, by comparing the η_V of the electrospray with and without 200-Guass magnetic field, Fig 14, we concluded that the application of a magnetic field consistently increased the energy of the primary population for various flowrates and extraction potentials within the stability regime of all ILFF propellants. The magnetic field also increased in the $\langle \epsilon_{ion} \rangle$ of the secondary population when it appeared in the RPA trace, Fig. 15.

The beam energy of the primary population for the IF-CES operating on the ILFF-30 propellant was most affected by the magnetic field compared to ILFF-20 or ILFF-40 propellants. At lower flowrates, the magnetic field consistently increased the primary population energy by more than 10-percent when compared to spray during a 0-Gauss magnetic field. The fact that the magnetic influence affected the beam energy of the ILFF-30 electrosprays the most was interesting as the magnetic influence on the beam divergence was also the largest when using the ILFF-30 propellant. This could mean for the specific wt% of NPs in ILFF-30 propellant the magnetic susceptibility of the nanoparticles dominates other potential influences caused by the addition of NPs, *i.e.* changes in density, surface tension, conductivity and viscosity.

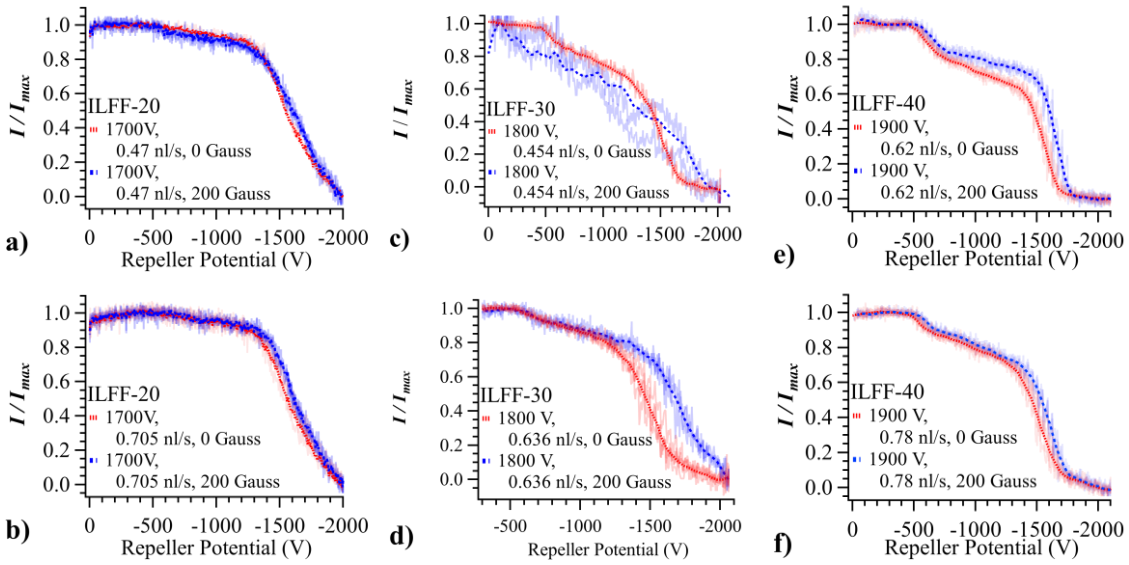

Figure 15. RPA traces of an electrospray acquired from the IF-CES with (blue) and without (red) a 200-Gauss magnetic field applied. Each trace shown here was an average of two RPA sweeps (light blue and light red). The propellants used are ILFF-20 operating at with V_{ext} = 1700 V, and flowrates, Q, of (a) 0.47 nl/s and (b) 0.705 nl/s; ILFF-30 operating with an V_{ext} = 1800 V and Q of (c) 0.454 and (d) 0.636 nl/s; and ILFF-40 with an V_{ext} = 1900 V and Q of (e) 0.62 and (f) 0.78 nl/s.

The general increase in the energy of both populations caused by the magnetic field application suggests that the emission site location of all charged particles reacted to the application of the magnetic field. The shape of the Taylor cone that formed during ILFF electrospray emission was already observed to change significantly, Fig. 11. Therefore, it is likely this effect that the shape change induced the increase in most probable ion energy, though the specific mechanism was not determined in this study.

VII. Conclusions

The divergence and energy of an electrospray beam from an electrospray source was measured while the source operated on the neat IL EMIM-NTf2 and three solutions of an ILFF. The parent ILFF was comprised of 26.0 wt% iron oxide NPs, 4.6 wt% copolymer, and 69.4 wt% EMIM-NTf2. The solutions of ILFF were produced by adding 20, 30 and 40 %(v/v) to the neat IL which resulted in nanoparticle concentrations of 3.04, 5.98, 8.80, and 14.15 wt%, respectively. The beam divergence and beam energy was measured for the same capillary source, running on the same four propellants, while subjected to a 200-Gauss magnetic field concentrically aligned with the capillary needle; the magnetic field was produced using a Helmholtz coil to create a gradient-free field within its the hollow core. The beam divergence and beam energy of the source were shown to be dependent on two new variables, the nanoparticle concentration and the applied magnetic field.

The NPs influenced both the beam divergence and beam energy of the neat IL electrospray. The current density at higher half-angles of the ILFF-30 and ILFF-40 electrosprays (higher wt% NPs) was significantly higher than electrosprays of neat IL or ILFF-20 propellants. Furthermore, the percent of the electrospray beam not intercepted by the extractor plate was significantly less for the ILFF-30 and ILFF-40 propellants. These two observations led us to conclude propellants with higher wt% NPs produced broader electrospray beams.

The beam divergence efficiency, η_B, was not determined from the current density profile of the IL electrospray nor any of the ILFF propellants, due to the poor angular resolution. However, η_B could be determined in future experiments by using a Faraday stack with more plates, or creating a setup that provides rotation of both the electrospray source and magnetic field source relative to the diagnostic tools.

The electrosprays of ILFF-30 and ILFF-40 propellants had $\langle \epsilon_{ion} \rangle$ that were consistently lower, relative to the extraction potential, than those of the neat IL and ILFF-20 electrosprays. Furthermore, a second energy population was recorded for the electrosprays using propellants with higher wt% NPs, and was 30% to 50% of the extraction potential.

The effect magnetic stress had on the beam divergence was only statistically significant for ILFF-20 and ILFF-30 propellants. When applied, the magnetic field either broadened or tightened the beam depending on the propellant, flowrate, and extraction potential. The most significant results were measured while running the ILFF-20 propellant at 0.47 nl/s and 1600 V, where the application of the magnetic field increased the fraction of the current in the center of the beam by a summed total of 25 percent.

Magnetic stress had a significant effect on the $\langle \epsilon_{ion} \rangle$ of the emitted species from the IF-CES operating on the ILFF propellants. The $\langle \epsilon_{ion} \rangle$ was generally increased for all three propellants, and the mean energy of the secondary population increased when it appeared in the RPA traces. Electrosprays of ILFF-30 were most affected, increasing by upwards of 16 percent for multiple operating conditions.

Acknowledgments

KJT would like to thank Marty Toth and Bill Langdon for machining all custom components for the experiments. All authors would to thank the US Air Force Office of Scientific Research: International AOARD and Sirtex Medical Limited for funding the development of the ILFFs, Nirmesh Jain and Brian Hawkett for the synthesis of the ILFFs, and Steve Jones and Stephanie Bickley for designing and preparing the monodomain magnetic particles. The material is based upon work supported by NASA under award No NNX13AM73H. Any opinions, findings, and conclusions or recommendations expressed in this material are those of the authors and do not necessarily reflect the views of the National Aeronautics and Space Administration.

References

1. Wright, W.P. and P. Ferrer, *Electric micropropulsion systems.* Progress in Aerospace Sciences, 2015. **74**(Supplement C): p. 48-61.
2. Leomanni, M., et al., *Propulsion options for very low Earth orbit microsatellites.* Acta Astronautica, 2017. **133**(Supplement C): p. 444-454.
3. Lemmer, K., *Propulsion for CubeSats.* Acta Astronautica, 2017. **134**(Supplement C): p. 231-243.
4. Gamero-Castaño, M. and V. Hruby, *Electrospray as a Source of Nanoparticles for Efficient Colloid Thrusters.* Journal of Propulsion and Power, 2001. **17**(5): p. 977-987.
5. Alexander, M.S., et al., *Electrospray Performance of Microfabricated Colloid Thruster Arrays.* Journal of Propulsion and Power, 2006. **22**(3): p. 620-627.
6. Lozano, P.C., M. Martínez-Sánchez, and V. Hruby, *Electrospray Propulsion*, in *Encyclopedia of Aerospace Engineering*2010, John Wiley & Sons, Ltd.
7. Prince, B.D., B.A. Fritz, and Y.-H. Chiu, *Ionic Liquids in Electrospray Propulsion Systems*, in *Ionic Liquids: Science and Applications*2012, American Chemical Society. p. 27-49.
8. Arestie, S., C. Whitlock, and P.C. Lozano, *Ion Electrospray Propulsion System Feasibility Study for various Satellite Missions and Architectures*, in *49th AIAA/ASME/SAE/ASEE Joint Propulsion Conference*2013, American Institute of Aeronautics and Astronautics.
9. Earle, M.J. and K.R. Seddon, *Ionic liquids. Green solvents for the future*, in *Pure and Applied Chemistry*2000. p. 1391.
10. MacFarlane, D.R., et al., *Ionic liquids based on imidazolium, ammonium and pyrrolidinium salts of the dicyanamide anion.* Green Chemistry, 2002. **4**(5): p. 444-448.
11. Lozano, P. and M. Martínez-Sánchez, *Ionic liquid ion sources: suppression of electrochemical reactions using voltage alternation.* Journal of Colloid and Interface Science, 2004. **280**(1): p. 149-154.
12. Jackson, G.P. and D.C. Duckworth, *Electrospray mass spectrometry of undiluted ionic liquids.* Chemical Communications, 2004. **0**(5): p. 522-523.
13. *Effect of liquid properties on electrosprays from externally wetted ionic liquid ion sources.* Journal of Applied Physics, 2007. **102**(9): p. 094310.
14. Krpoun, R. and H. Shea, *Microfabricated out-of-plane arrays of integrated capillary nano-electrospray emitters*, in *Transducers 2009*2009: Denver, CO, USA. p. 1242-1245.
15. Borner, A., Z. Li, and D.A. Levin, *Modeling of an ionic liquid electrospray using molecular dynamics with constraints.* The Journal of Chemical Physics, 2012. **136**(12): p. 124507-11.
16. Lenguito, G., J. Fernandez De La Mora, and A. Gomez, *Scaling up the power of an electrospray microthruster.* Journal of Micromechanics and Microengineering, 2014. **24**(5): p. 055003.
17. Miller, S.W., *ANALYSIS OF ION EMITTING JET STRUCTURES DURING IONIC LIQUID ELECTROSPRAYING*, in *AEROSPACE ENGINEERING*2015, MISSOURI UNIVERSITY OF SCIENCE AND TECHNOLOGY: Rolla, MO.
18. Gamero-Castaño, M., *The Expansion of Colloid Thruster Beams and its Dependence on Emission Temperature*, in *49th AIAA/ASME/SAE/ASEE Joint Propulsion Conference*2013, American Institute of Aeronautics and Astronautics.
19. Nabity, J.A. and J.W. Daily, *Effect of Ionic Liquid Composition on Colloid Thruster Emission and Thrust Performance.* Journal of Propulsion and Power, 2017: p. 0-0.

20. Meyer, E.J., Lyon B. King. *Electrospray from an Ionic Liquid Ferrofluid utilizing the Rosensweig Instability* in *49th AIAA/ASME/SAE/ASEE Joint Propulsion Conference & Exhibit*. 2013. San Jose, CA.
21. King, L.B., *Ferroelectrohydrodynamics of ionic liquid ferrofluid surface instabilities and jets*, in *50th AIAA/ASME/SAE/ASEE Joint Propulsion Conference & Exhibit*2014: Cleveland, OH.
22. Jackson, B.A., *Characterization of an Ionic Liquid Ferrofluid Electrospray Emission Pattern*, in *50th AIAA/ASME/SAE/ASEE Joint Propulsion Conference & Exhibit*2014: Cleveland, OH.
23. Meyer IV, E.J., *Development of an Ionic Liquid Ferrofluid Electrospray Source and Mode Shape Studies of a Ferrofluid in a Non-uniform Magnetic Field*, in *Mechanical Engineering - Engineering Mechanics*2014, Michigan Technological University: Houghton, MI.
24. Terhune, K.J., et al., *The effects of magnetic surface stress on electrospray of an ionic liquid ferrofluid*, in *52nd AIAA/SAE/ASEE Joint Propulsion Conference*2016: Salt Lake City, UT.
25. Terhune, K.J., et al., *Species measurements in the beam of an ionic liquid ferrofluid capillary electrospray source under magnetic stress*, in *52nd AIAA/SAE/ASEE Joint Propulsion Conference*2016: Salt Lake City, UT.
26. Jackson, B.A., K.J. Terhune, and L.B. King, *Ionic liquid ferrofluid interface deformation and spray onset under electric and magnetic stresses.* Physics of Fluids, 2017. **29**(6): p. 064105.
27. Madden, A., et al., *Effect of a homogeneous magnetic field on the electrospraying characteristics of sulfolane ferrofluids*, 2016, Yale University.
28. Boudouvis, A.G., et al., *Normal field instability and patterns in pools of ferrofluid.* Journal of Magnetism and Magnetic Materials, 1987. **65**(2–3): p. 307-310.
29. Lozano, P.C., *Studies on the Ion-Droplet Mixed Regime in Colloid Thrusters*, in *Department of Aeronautics and Astronautics*2003, Massachusetts Institute of Technology: Cambridge.
30. Miller, S.W., et al., *Electrospray of 1-Butyl-3-Methylimidazolium Dicyanamide Under Variable Flow Rate Operations.* Journal of Propulsion and Power, 2014: p. 1-10.
31. Gassend, B., et al., *A Microfabricated Planar Electrospray Array Ionic Liquid Ion Source With Integrated Extractor*. Microelectromechanical Systems, Journal of, 2009. **18**(3): p. 679-694.
32. Hutchinson, I.H., *Principles of Plasma Diagnostics*. 2 ed2002, Cambridge: Cambridge University Press.
33. Miller, C.E. and P.C. Lozano, *Measurement of the Fragmentation Rates of Solvated Ions in Ion Electrospray Thrusters*, in *52nd AIAA/SAE/ASEE Joint Propulsion Conference*2016: Salt Lake City, UT.
34. Chiu, Y.-H., et al., *Mass Spectrometric Analysis of Colloid Thruster Ion Emission from Selected Propellants.* Journal of Propulsion and Power, 2005. **21**(3): p. 416-423.
35. Chiu, Y.-H., et al., *Mass Spectrometric Analysis of Ion Emission for Selected Colloid Thruster Fuels*, in *39th AIAA/ASME/SAE/ASEE Joint Propulsion Conference and Exhibit*2003, American Institute of Aeronautics and Astronautics: Huntsville, Alabama.
36. Miller, S.W., et al., *Mass Spectrometry of Selected Ionic Liquids in Capillary Electrospray at Nanoliter Volumetric Flow Rates*, in *52nd AIAA/SAE/ASEE Joint Propulsion Conference*2016: Salt Lake City, UT.
37. Miller, S.W., B.D. Prince, and J.L. Rovey. *Capillary Extraction of the Ionic Liquid [Bmim][DCA] for Variable Flow Rate Operations*. in *48th AIAA/ASME/SAE/ASEE Joint Propulsion Conference & Exhibit*. 2012. Atlanta, Georgia: AIAA.
38. Chiu, Y.H., et al., *Vacuum electrospray ionization study of the ionic liquid, [Emim][Im]*. International Journal of Mass Spectrometry, 2007. **265**(2–3): p. 146-158.
39. Fröba, A.P., H. Kremer, and A. Leipertz, *Density, Refractive Index, Interfacial Tension, and Viscosity of Ionic Liquids [EMIM][EtSO4], [EMIM][NTf2], [EMIM][N(CN)2], and [OMA][NTf2] in Dependence on Temperature at Atmospheric Pressure.* The Journal of Physical Chemistry B, 2008. **112**(39): p. 12420-12430.
40. Leys, J., et al., *Temperature dependence of the electrical conductivity of imidazolium ionic liquids.* The Journal of Chemical Physics, 2008. **128**(6): p. 064509.
41. Fredlake, C.P., et al., *Thermophysical Properties of Imidazolium-Based Ionic Liquids.* Journal of Chemical & Engineering Data, 2004. **49**(4): p. 954-964.
42. Morad, M.R., et al., *A Very Stable High Throughput Taylor Cone-jet in Electrohydrodynamics.* 2016. **6**: p. 38509.
43. Jackson, B.A. and B.K. Lyon. *Time Resolved Divergence Mapping and Long Duration Emission Studies of an Ionic Liquid Ferrofluid Electrospray Source*. in *35th International Electric Propulsion Conference*. 2017. Atlanta, Georgia, USA.
44. Lozano, P.C., *Energy properties of an EMI-Im ionic liquid ion source.* Journal of Physics D: Applied Physics, 2006. **39**(1): p. 126.
45. Gamero-Castaño, M., *Characterization of the electrosprays of 1-ethyl-3-methylimidazolium bis(trifluoromethylsulfonyl) imide in vacuum.* Physics of Fluids, 2008. **20**(3): p. 032103.